Directional coupler based on radiatively coupled waveguides

M. Shamonin, M. Lohmeyer and P. Hertel

Department of Physics, University of Osnabrück

Barbarastraße 7, D-49069 Osnabrück, Germany

Abstract

We investigate a system of two waveguides with leaky modes sharing a common substrate (radiatively coupled waveguides). The main advantage of such a system is the possibility of remote coupling. A perturbation theory is developed for both TE- and TM-polarization. Numerical calculations of dispersion curves and of the coupling length allow to determine the limitations of the perturbation theory. The influence of multimode interference on the process of beating is studied by considering the propagation of a given initial field. Finally, a new design for an effective integrated optical TE/TM polarization splitter is proposed.

Keywords: integrated optics, directional couplers, radiatively coupled waveguides, polarization splitters

1. INTRODUCTION

Directional couplers have many applications in the field of integrated optics and optoelectronics, such as switches, power dividers, filters, or modulators[1–4]. The conventional principle of coupling is based on the existence of evanescent mode fields outside the waveguides. In this case, the coupling coefficient falls off exponentially with the separation distance, and an acceptable coupling length can be achieved only if the waveguides are sufficiently close. This complicates the realization of devices based on coupled waveguides. Remote coupling can be achieved by using antiresonant reflecting optical waveguide (ARROW) structures[5–8]. Recently a possibility of remote coupling in a system of two waveguides with leaky modes sharing a substrate (see Fig. 1), the so-called radiatively coupled waveguides, was demonstrated[9]. We believe that such a system is worth considering it for integrated optical applications. The purpose of this paper is to theoretically investigate a system of two radiatively coupled waveguides in detail.

The paper is organized as follows. Section 2 explains the operation principle of radiatively coupled waveguides. In section 3 a perturbation theory of radiatively coupled waveguides is developed for both TE- and TM-polarized modes. Numerical investigations in section 4 allow to determine the regions of applicability of the perturbation theory and to gain further insight into the properties of radiatively coupled waveguides. The influence of multimode interference on the coupling process is studied in section 5 by analyzing the propagation of a given initial field. Finally, in section 6 we propose a new design for an effective integrated optical TE/TM polarization splitter.

2. RADIATIVELY COUPLED WAVEGUIDES

Consider two identical slab waveguides to be coupled. Each waveguide consists of a film (refractive index n_1) of thickness h sandwiched between a cover (refractive index n_0) and a substrate (refractive index n_2) (see Fig. 1a). It carries a guided mode with an effective mode index n^*. In the following we consider both TE and TM polarizations. Fig. 1

The conventional coupling of spatially separated but optically coupled waveguides is based on the existence of evanescent mode fields outside the guides. The refractive index of the medium in the coupling region is smaller than the effective mode index. For radiatively coupled waveguides, as shown in Fig. 1c, the refractive index n_3 in the coupling region is larger than the mode index. We call this radiative coupling due to two reasons. First, the modes of individual waveguides are leaky and radiate power into the surrounding medium with a large refractive index n_3 (see Fig. 1b). Second, similarly to radiation modes, the mode fields of interest show oscillatory behavior along the x-axis in the coupling region. The entire structure is a multimode multilayered waveguide, and its guided (bound) modes have no radiation losses. Figure 2 shows mode profiles for typical waveguide parameters taken from Ref. 10. The symmetric and antisymmetric modes of interest (TM_{14} and TM_{15} in Fig. 2) are not the fundamental modes of the entire structure, but those with mode indices n_s and n_a closest to the mode index n^* of a basic slab waveguide. Contrary to other modes, these two modes have small wave amplitudes inside the central layer (see Fig. 2), and their superposition matches the mode field of a basic slab waveguide well. Therefore, one can expect that in the case of excitation at the end of one waveguide, mainly these two modes will be important. Since they have different propagation constants, it is expected that after a distance equal to Fig. 2

$$L_c = \frac{\lambda}{2\left|n_s - n_a\right|} \tag{1}$$

the radiation will be transferred from the first to the second waveguide. λ stands for the operation wavelength. We call L_c the coupling length, although L_c and the real distance after which the radiation is transferred from one waveguide to another can be different. Obviously, L_c, as defined by Eq.(1), has its physical significance only when the coupling process is dominated by only two modes, symmetric and antisymmetric[8]. However, one can always formally define L_c as in Eq.(1) assuming that n_s and n_a are the effective mode indices of symmetric and antisymmetric modes closest to n^*.

Figure 3a shows dispersion curves for typical waveguide parameters. Obviously, the mode spectrum is enriched for thicker central layers. The propagation constants of the modes of interest lie between n_1 and n_2 likewise for the basic slab waveguide. This region is shown enlarged in Fig. 3b. The behavior of the dispersion curves in Fig. 3b is remarkably similar to an ARROW-coupler (compare Fig. 3b with Fig. 2b of Ref. 7). Fig. 3

3. PERTURBATION THEORY

If the thickness t of the buffer layer is sufficiently large ($A = \exp[-2k(n^{*2} - n_2^2)^{1/2} t] \ll 1$) one can consider the presence of medium 3 as a perturbation to the basic slab waveguide[10] and obtain the effective indices of the symmetric and antisymmetric TM-modes of interest as corrections to the mode index n^* of the basic slab waveguide:

$$n_{s,a} = n^* + \Re\mathrm{e}(\delta n_{lk}) + \delta n_{s,a}\,, \tag{2}$$

with

$$\delta n_{lk} = \frac{2\eta_1\eta_2 N_1^2 |N_2| A}{(\eta_1^2 N_1^2 + \eta_2^2|N_2|^2)(\eta_3^2 N_3^2 + \eta_2^2 |N_2|^2) n^* k h_{\mathrm{eff}}} [\eta_2^2|N_2|^2 - \eta_3^2 N_3^2 + 2\mathrm{i}\eta_2\eta_3 N_3 |N_2|]\,, \tag{3}$$

$$\delta n_{s,a} = \frac{4A\,\eta_1\eta_2^2\eta_3 N_1^2 |N_2|^2 N_3}{(\eta_3^2 N_3^2 + \eta_2^2|N_2|^2)(\eta_1^2 N_1^2 + \eta_2^2|N_2|^2) n^* k h_{\mathrm{eff}}} \tan\left(\frac{\theta_{s,a}}{2} + \psi\right)\,, \tag{4}$$

where

$$\begin{aligned}
h_{\mathrm{eff}} &= h + \frac{\eta_0}{k\eta_1|N_0|}\frac{N_1^2 + |N_0|^2}{N_1^2 + (\eta_0|N_0|/\eta_1)^2} + \frac{\eta_2}{k\eta_1|N_2|}\frac{N_1^2 + |N_2|^2}{N_1^2 + (\eta_2|N_2|/\eta_1)^2}\,,\\
\psi &= \tan^{-1}(\eta_3 N_3/\eta_2|N_2|)\,,\\
\theta_s &= kN_3H\,, \quad \theta_a = kN_3H + \pi\,,\\
N_i &= [n_i^2 - n^{*2}]^{1/2} \quad (i = 0, ..., 3)\,,\\
\eta_i &= n_i^{-2} \quad (i = 0, ..., 3)\,.
\end{aligned} \tag{5}$$

Here k is the wavenumber in vacuum and h_{eff} is the effective waveguide thickness[11]. δn_{lk} is the correction to n^* due to the finite thickness of the buffer layer 2 (see Fig. 1b). In this case the real part of δn_{lk} gives the change of the mode index due to the leakage, while $\Im\mathrm{m}(\delta n_{lk})$ determines the radiation loss coefficient α_{rad} of a leaky mode[12]:

$$\alpha_{rad} = k \, \Im\mathrm{m}(\delta n_{lk}) \, . \tag{6}$$

$\delta n_{s,a}$ are additional corrections for symmetric and antisymmetric solutions. The derivation of Eqs.(2)-(5) is explained in the Appendix. Previously published results for TE modes[10] can be obtained by substituting $\eta_{\mathrm{i}} \to 1$ $(\mathrm{i} = 0, ..., 3)$.

Formulas (3) and (4) are rather complicated. However, already a first look at them allows us to draw important conclusions. First, it can be seen that due to the tan-function in (4), the perturbation theory predicts a periodical dependence of $n_{s,a}$ on H. This result is at least qualitatively confirmed by Figure 3b, and we shall see below that there is quantitative agreement as well. Second, the perturbation theory breaks down if $(\theta_{s,a}/2 + \psi) \sim \pi/2 + \pi m$ (m is integer), since then $\delta n_{s,a} \to \infty$. This condition provides the quantitative criterion for regions where three modes have to be considered such that two-mode approximation is definitely invalid[8].

4. DISPERSION CURVES: COMPARISON OF ANALYTICAL AND NUMERICAL RESULTS

The theory presented in the previous section is an approximation. It is aimed at describing modes with propagation constants only slightly different from n^*. In this section we investigate the region of applicability of the perturbation theory in more detail. This is achieved by comparing the dispersion curves and the coupling length as calculated by using formula (2) and numerically. The result is depicted in Figure 4 for two different regions Fig. 4 of the variation of the thickness H. The perturbation theory works very well for index variations $|n_{s,a} - n^*| < 0.01$ in the region $H \leq 5$ μm, while for larger H the differences become clearly pronounced. The comparison for L_c is given in Fig. 5 . The perturbation theory predicts a periodical dependence on H. The numerical calculations show an almost periodical dependence on H, and the maximum of L_c within one period grows with H. The coupling process is best described by two modes[8] in the regions close to the local maxima of $L_c(H)$-curves. The conclusion to be drawn from comparing perturbation theory and numerical results is apparent: the perturbation theory provides good results for small thicknesses of the central layer and its applicability deteriorates with the growth of H. The application of the perturbation theory to the case of very thick central layers (e.g. $H \approx 95\,\mu$m[10]) seems to be unjustified. Fig. 5

5. INFLUENCE OF MULTIMODE INTERFERENCE ON THE COUPLING PROCESS

As was already seen in Fig. 3, the system of radiatively coupled waveguides can support many modes. Real initial fields can not always be well represented as a superposition of only two modes. Therefore, an excitation in just one of the outer sections unavoidably leads to several modes being excited. Assume that the fundamental mode of the basic slab waveguide is launched as an initial field into the section 1 (WG1). Such an experimental situation was realized in Ref. 10. The optical power carried by the mode is normalized to unity. To calculate the propagation of the initial field we use a Propagating-Mode Analysis (PMA)[13,14] based on the expansion of the propagating fields into the local modes of structure:

$$F(x,z) = \sum_m c_m \, \mathcal{F}_m(x) \exp \mathrm{i}\beta_m z \, , \tag{7}$$

where c_m is the amplitude of mode m and F the principal electric (TE) or magnetic (TM) field component. The mode field profile $\mathcal{F}_m(x)$ is normalized, such that $|c_m|^2$ is the power carried by the mode. In all our calculations the initial field was very well represented by such a superposition : $1 > \sum_m |c_m|^2 \geq 0.98$.

The accuracy and reliability of the PMA calculations were controlled with the finite-difference Beam-Propagation Method[15,16] (BPM). The results of the PMA and BPM calculations agreed well, since the amount of initially radiated power was very low. The PMA is significantly faster than the BPM, especially for large thicknesses of the central layer when a large number of points is required to simulate the oscillatory behavior correctly. Additionally, the PMA generates exact multimode interference patterns for arbitrary distances.

During propagation the optical power is transferred from the first waveguide to the second. Therefore, it is concentrated not only in the outer sections but also in the central layer. To evaluate the power in the outer sections we work out the overlap integrals with the fundamental modes of these waveguides:

$$P_1(z) = |(F(x,z),\, \phi_1(x))|^2 \,, \quad P_2(z) = |(F(x,z),\, \phi_2(x))|^2 \,, \tag{8}$$

where ϕ_1 and ϕ_1 are normalized mode fields in sections 1 (denoted as WG1 in Fig. 1c) and 2 (denoted as WG2), respectively. $(F,\, \phi)$ stands for the proper scalar product for each polarization state[17]. The total optical power in outer sections $P = P_1 + P_2$ is a measure of "useful" power which can be coupled out of the system.

Figure 6 shows the variation of the power in sections 1 and 2 as well as of the total power $P_1 + P_2$ with the propagation distance z for different thicknesses of the central layer. These thicknesses were chosen in such a way that the theoretical coupling length calculated from the perturbation theory was 1 mm. It is seen that for thin ($H < 5$ μm) central layers the physical situation is excellently described by the coupling of only two modes. For thick ($H \sim 20$ μm) layers multimode interference results in a complicated picture of intermode beating. The distance after which the power is transferred form the first waveguide to the second is larger than 1 mm. In general, a sizeable amount of power can be contained in the central layer and therefore cannot be coupled out of the system if the device length is not properly chosen. The power contained in the central layer at the output of the device plays Fig. 6

the role of intrinsic losses of the system.

Note that although the entire mode spectrum is excited, only a small number of modes whose propagation constants are close to n^* determine the propagation picture. This is illustrated in Fig. 7 . It is seen that the interference of the four main modes (TM_{21} - TM_{24}) is practically indistinguishable from the case when all modes were taken into account (compare Figs. 6c and 7c). Fig. 7

6. APPLICATION: TE/TM POLARIZATION SPLITTER

There is a growing interest in new concepts for integrated optical polarization splitting devices[18–23]. We propose to use radiatively coupled waveguides for the design of a TE/TM mode splitter[24]. The device is based on the difference in the beat length of the two polarization states (see e.g. Fig. 5). To estimate the required waveguide parameters the perturbation theory is used. The maximum coupling length L_c^{max} is inversely proportional to the optical loss coefficient α_{rad}[10], and the splitter operates close to this maximum. α_{rad} can be calculated with the help of Eqs. (3) and (6). The waveguide parameters are selected in such a way that $L_c^{max,TM}/L_c^{max,TE} = \alpha_{rad}^{TE}/\alpha_{rad}^{TM} = 0.8$. Therefore, it is expected that after 5 half-beat lengthes of the TM-polarized waves (or, equivalently, 4 half-beat lengthes of TE-polarized waves) the different polarization states will be directed into different output channels (see Fig. 8) . Fig. 8

Very strict fabrication tolerances with respect to the waveguide thickness are a general property of all polarization splitting devices[22]. To evaluate the performance of the proposed polarization splitter and to estimate the allowed fabrication tolerances, we calculate the extinction ratios ER_1 and ER_2[21,22]:

$$ER_1 = 10 \log_{10} \frac{P_1^{TM}}{P_1^{TE}} \qquad \text{and} \qquad ER_2 = 10 \log_{10} \frac{P_2^{TE}}{P_2^{TM}} \, . \tag{9}$$

Figure 9 shows the variation of the extinction ratios ER_1 and ER_2 with the propagation Fig. 9

distance z. For a good polarization discrimination the device length should be chosen in such a way that both extinction ratios are below -20 dB (or above +20 dB)[22]. These levels are shown by dashed lines.

Table 1 gives values of the device length L_{ps} and the allowed fabrication tolerance for the thickness of the central layer corresponding to different values of H. Remaining waveguide parameters are as in Fig. 8. Since L_c varies almost periodically with H, there is also an almost periodical set of possible values of H, where the polarization discrimination occurs. For the used waveguide parameters these possible values of H can be expressed by $H \approx (0.661 + n \cdot 0.411)$ μm ($n > 0$ is integer). Table 1 shows the allowed tolerances for three typical values of H. The general trend is that the allowed tolerances for H improve for smaller H. At the same time, the required tolerances for h and t are practically independent of H and are approximately equal to 10 nm (see Fig. 10). The tolerance $\pm$ 40 μm for L_{ps} also remains constant.

Tab. 1

Fig.10

A tolerance of $\pm$ 10 nm is a significant improvement if compared with $\pm$ 1 nm as required for the design of Thyagarajan et al.[21]. A recently proposed ARROW structure design[22] is slightly less critical ($\pm$ 15 nm), but more complicated, since it contains more layers. The allowed tolerances in the proposed structure are reasonable and better than for polarization splitters based on asymmetric conventional waveguides[22]. The search for waveguides with other technologically feasible sets of parameters and improved fabrication tolerances seems to be promising.

7. CONCLUSIONS

- A system of two radiatively coupled waveguides, when the modes of the individual waveguides are leaky, has been studied in detail. The main advantage of such a system over the conventional directional coupler is that coupling between rather remote channels can be achieved.

- Approximate expressions for the effective mode indices of the two (symmetric and antisymmetric) modes of interest are presented for both TE- and TM-polarizations. This perturbation theory works very well for sufficiently thin central layers. It allows to conveniently design a TE/TM mode splitter. For thick central layers, numerical calculations have to be used. An application of the perturbation theory to extremely remote ($H \sim 100$ μm) waveguides is unfounded.

- Although coupling between two remote channels is possible, multimode interference leads to a complicated picture of beating during the propagation.

- We propose an integrated optical TE/TM polarization splitter based on radiatively coupled waveguides. Our device is as efficient as the three-waveguide splitter of Thyagarajan et al.[21], but the fabrication tolerances in comparison with the latter design are considerably improved. Although the required tolerances are somewhat smaller than in a recent proposal by Trutschel et al.[22], our design is considerably simpler because it consists of only a few layers.

ACKNOWLEDGMENTS

Financial support by Deutsche Forschungsgemeinschaft, Sonderforschungsbereich 225 is gratefully acknowledged. We thank H. Dötsch for critically reading of the manuscript and A. Erdmann for participation in the early stage of this project.

APPENDIX

Assuming harmonic time dependence of the form $\exp(-\mathrm{i}\omega t)$ the mode magnetic field in a layer l can be represented as a sum of upward and downward traveling waves

$$H_y = a_l^- \cdot \{\exp[-\mathrm{i}kN_l(x-x_l)] + R_l \exp[\mathrm{i}kN_l(x-x_l)]\} \exp(\mathrm{i}kn^* z)\,,$$

where $N_l = (n_l^2 - n^{*2})^{1/2}$. If $n^* > n_l$ we must replace N_l by $\mathrm{i}|N_l|$.

R_l are the reflection coefficients of the TM waves at the surface $x = x_l$. In multilayered structures they are related by the following recursion formula:

$$R_l = \frac{\eta_l N_l(1+R_{l+1}) - \eta_{l+1}N_{l+1}(1-R_{l+1})}{\eta_l N_l(1+R_{l+1}) + \eta_{l+1}R_{l+1}(1-R_{l+1})} \exp 2\mathrm{i}kN_l h_l\,, \tag{10}$$

where $\eta_l = n_l^{-2}$ and $h_l = x_l - x_{l+1}$.

First, we consider the slab waveguide of Fig. 1a as an unperturbed structure. Application of boundary conditions to the TM mode field yields the well-known dispersion equation:

$$D = \eta_0 N_0(1+R_1) + \eta_1 N_1(1-R_1) = 0\,.$$

To find δn^* in the framework of perturbation theory, we demand that the variation of D vanishes, $\delta D = (\eta_0 N_0 - \eta_1 N_1)\delta R_1 + (\partial D/\partial n^*)\delta n^* = 0$. After some algebra we obtain the following correction to n^* due to the change δR_1 in the reflection coefficient R_1 caused by the presence of the central layer:

$$\delta n^* = \frac{N_1}{2\mathrm{i}n^* k h_{\mathrm{eff}}} \frac{\eta_1 N_1 - \eta_0 N_0}{\eta_1 N_1 + \eta_0 N_0} \delta R_1\,. \tag{11}$$

The entire system of radiatively coupled waveguides is symmetric, thus $R_3 = \exp(\mathrm{i}\theta_{s,a})$ with $\theta_s = kN_3H$, $\theta_a = kN_3H + \pi$ for symmetric (s) and antisymmetric (a) modes of interest. The known values of R_3 allow to calculate δR_1 using the relationship (10) and to obtain the corrections $\delta n_{s,a}$ from (11).

FIGURES

Fig. 1. A basic slab waveguide (a) and a slab waveguide with leaky modes (b) are shown. If two waveguides with leaky modes share a substrate they form radiatively coupled waveguides (c). Note that the refractive index n_3 of the central layer is larger than the effective index of the waveguide mode n^*. Arrows illustrate the power flow. $H = 0$ corresponds to conventionally coupled waveguides.

Fig. 2. Field profiles of some TM-modes for two radiatively coupled waveguides. The fields are normalized as $\int \epsilon^{-1}|H_y|^2\, dx = 1$. Parameters $n_0 = 1, n_1 = 1.49, n_2 = 1.46, n_3 = 1.52, h = 1.35$ μm, $t = 0.8$ μm and $\lambda = 0.6328$ μm are taken from Ref. 10. The thickness H of the central layer is 12.5 μm. The entire structure supports 61 TM-modes.

Fig. 3. (a) Effective mode index β/k of the TM-modes versus the thickness H of the central layer. Parameters are the same as in Fig. 2. (b) Part of the dispersion curves from (a). The modes are designated. Solid lines denote symmetric modes, dashed lines denote antisymmetric modes.

Fig. 4. Effective mode index β/k of the TM-modes as calculated using the perturbation theory (solid lines) and numerically (dashed lines) versus the thickness H of the central layer for different regions of the variation of H: $0 \leq H \leq 5$ μm (a) and $15 \leq H \leq 20$ μm (b). Only the effective mode indices close to $n^* = 1.4789$ are shown. Parameters are the same as in Fig. 2.

Fig. 5. Coupling length L_c of TM and TE modes as calculated using the perturbation theory (solid lines) and numerically (dashed lines) versus the thickness H of the central layer for different regions of the variation of H: $0 \leq H \leq 5$ μm (a) and $15 \leq H \leq 20$ μm (b). The maximal coupling length L_c^{max} according to the perturbation theory is shown. Parameters are the same as in Fig. 2.

Fig. 6. Power P_1 (solid lines), P_2 (dashed lines) of TM-waves in WG1 and WG2, respectively, and the total power $P_1 + P_2$ (dotted lines) versus the propagation distance z for different values of the central layer thickness H. Note that the given values of H correspond to the same value of $L_c^{TM} = 1$ mm accordingly to the perturbation theory. The total number of modes supported by the entire structure increases with H. The structure supports 15, 32 and 87 TM-modes, respectively. Parameters are the same as in Fig. 2.

Fig. 7. Power P_1 (solid lines), P_2 (dashed lines) of TM-waves in WG1 and WG2, respectively, and the total power $P_1 + P_2$ (dotted lines) versus the propagation distance z if a different number of propagating modes is taken into account. $H = 19.855$ μm, remaining parameters are the same as in Fig. 2.

Fig. 8. Propagation of the TE-polarized wave (a) in comparison to the propagation of the TM-polarized wave (b). The properly polarized mode of a basic slab waveguide was launched into WG1 at $z = 0$. Accordingly to the theoretical prediction, light with different polarization states is directed towards different output channels. Parameters are $n_0 = 1.51065$, $n_1 = 1.52$, $n_2 = 1.512$, $n_3 = 1.70$, $h = 1.50$ μm, $t = 0.77$ μm, $\lambda = 0.6328$ μm and $H = 10.108$ μm. The total length of the device is $L_{ps} = 4548$ μm.

Fig. 9. Extinction ratios ER_1, ER_2 versus the propagation distance z for the structure of Fig. 8.

Fig. 10. (a) Extinction ratios ER_1, ER_2 versus the thickness of the central layer H (a), the film thickness h (b) and the thickness t of the buffer layer (c). In each figure the remaining parameters are as in Fig. 8.

REFERENCES

1. H.F. Taylor, "Optical switching and modulation in parallel dielectric waveguides," J. Appl. Phys. **44**, 3257-3262 (1974)

2. H. Kogelnik and R.V. Schmidt, "Switched directional couplers with alternating $\Delta\beta$," IEEE J. Quantum Electron. **QE-12**, 396-401 (1976)

3. R.C. Alferness and R.V. Schmidt, "Tunable optical waveguide directional coupler filter," Appl. Phys. Lett. **33**, 161-163 (1978)

4. R.G. Hunsperger, *Integrated Optics: Theory and Technology* (Springer Verlag, Berlin, Heidelberg, 1982)

5. M.A. Duguay, Y. Kojubun, T.L. Koch, and L. Pfeiffer, "Antiresonant reflecting optical waveguide in SiO_2-Si multilayer structures," Appl. Phys. Lett. **49**, 13-15 (1986)

6. T. Baba and Y. Kokobun, "Dispersion and radiation loss characteristics of antiresonant reflecting optical waveguides – numerical results and analytical expression," IEEE J. Quantum Electron. **28**, 1689-1700 (1992)

7. M. Mann, U. Trutschel, C. Wächter, L. Leine and F. Lederer, "Directional coupler based on an antiresonant reflecting optical waveguide," Opt. Lett. **16**, 805-807 (1991)

8. F. Lederer, L. Leine, M. Mann, T. Peschel, R. Muschall, U. Trutschel, C. Wächter, C. Carigan, M.A. Duguay, and F. Ouelette, in *"Integrated Optics and Micro-Optics with Polymers"*, eds. G. Wegner, W. Karthe and W. Ehrfeld, 'Teubner-Texte zur Physik'-series, **27** (Teubner Verlagsgesellschaft, Stuttgart,1993) 301-331

9. V.L. Maslennikov, V.A. Sychugov, A.V. Tishchenko and B.A. Usievich, "Light generation in a system of two coupled waveguides," Sov. J. Quant. Electron. **22**, 1041-1044 (1992)

10. S.M. Loktev, V.A. Sychugov and B.A. Usievich, "Propagation of light in a system of

two radiatively coupled waveguides," Quantum Electron. **24**, 435-438, (1994)

11. M.T. Wlodarczyk and S.R. Seshadri, "Analysis of grating couplers for planar dielectric waveguides," J. Appl. Phys. **58**, 69-87 (1985)

12. This means that $n^* + \Re\mathrm{e}(\delta n_{lk})$ is the effective mode index of a waveguide with leaky mode shown in Fig. 1 (b), and α_{rad} is its leakage parameter.

13. G.J.M. Krijnen, *All-optical switching in nonlinear integrated optic devices*, PhD thesis, University of Twente, Enschede, The Netherlands, 1992 (ISBN: 90-9004929-0)

14. J. Willems, J. Haes and R. Baets, "The bidirectional mode expansion method for two-dimensional waveguides: the TM case," Opt. Quant. Electron. **27**, 995-1007 (1995)

15. Y. Chung and N. Dagli, "An assessment of finite difference beam propagation method," IEEE J. Quantum Electron. **26**, 1335-1339 (1990)

16. W. Huang, C. Xu, S.-T. Chu and S.K. Chaudhuri, "The finite-difference vector beam propagation method: analysis and assessment," J. Lightwave Technol. **LT-10**, 293-304 (1992)

17. W.H. Weber, S.L. McCarthy and G.W. Ford, "Perturbation theory applied to gain or loss in an optical waveguide," Appl. Opt. **13**, 715-716 (1974)

18. Y. Shani, C.H. Henry, R.C. Kistler and K.J. Orlowsky, "Four-port integrated optic polarization splitter," Appl. Opt. **29**, 337-339 (1990)

19. M. Eisenmann and E. Weidel, "Single-mode fused biconical coupler optimized for polarization beamsplitting," J. Lightwave Technol. **9**, 853-858 (1991)

20. K. Thyagarajan, S.D. Seshadri and A.K. Ghatak, "Waveguide polarizer based on resonant tunelling," J. Lightwave Technol. **LT-9** 315-317 (1991)

21. K. Thyagarajan and S. Pilevar, "Resonant tunelling three-waveguide polarization splitter," J. Lightwave Technol. **LT-10** 1334-1337 (1992)

22. U. Trutschel, F. Ouelette, V. Delisle, M.A. Duguay, G. Fogarty, and F. Lederer: "Polarization splitter based on antiresonant reflecting optical waveguides," J. Lightwave Technol. **LT-13**, 239-243 (1995)

23. X. Li and R.T. Deck, "Light polarizer based on antiresonant reflecting layers in a directional coupler", Appl. Phys. Lett. **66**, 130-132 (1995)

24. M. Shamonin, A. Erdmann and P. Hertel, "Properties of TE/TM polarized-mode propagation in a system of two radiatively coupled waveguides," European Optical Society, Annual Meetings Digest Series: Vol. 2A, "Photonics'95", 170-173 (1995)

Table 1.

H [nm]	L_{ps} [μm]	$\pm\Delta H$ [nm]
2305	4428	20
4361	4464	17
10108	4548	15

Figure 1

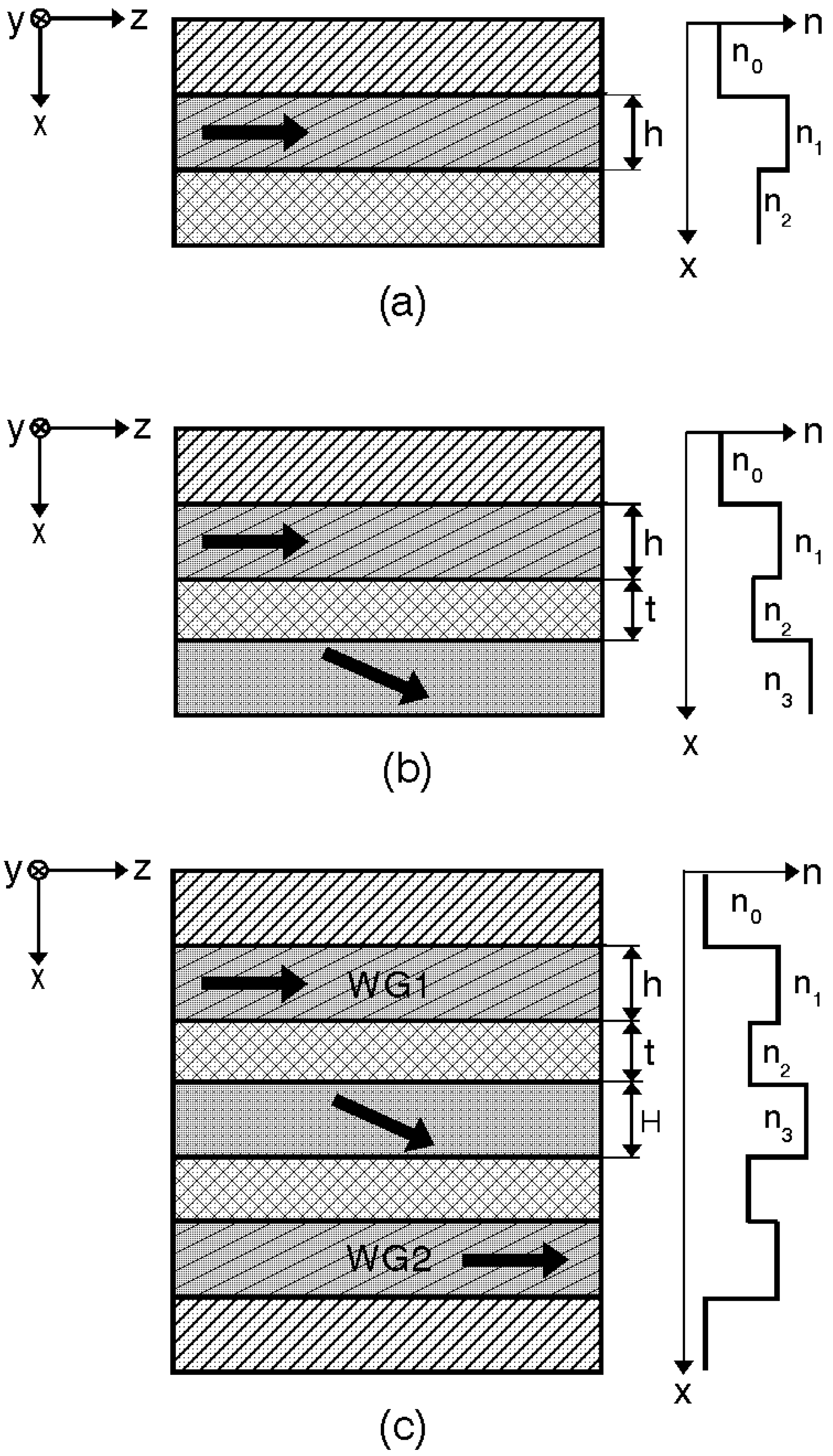
y
z
x
h
n
n0
n1
n2
x
(a)
y
z
x
h
t
n
n0
n1
n2
n3
x
(b)
y
z
x
WG1
WG2
h
t
H
n
n0
n1
n2
n3
x
(c)

Figure 2

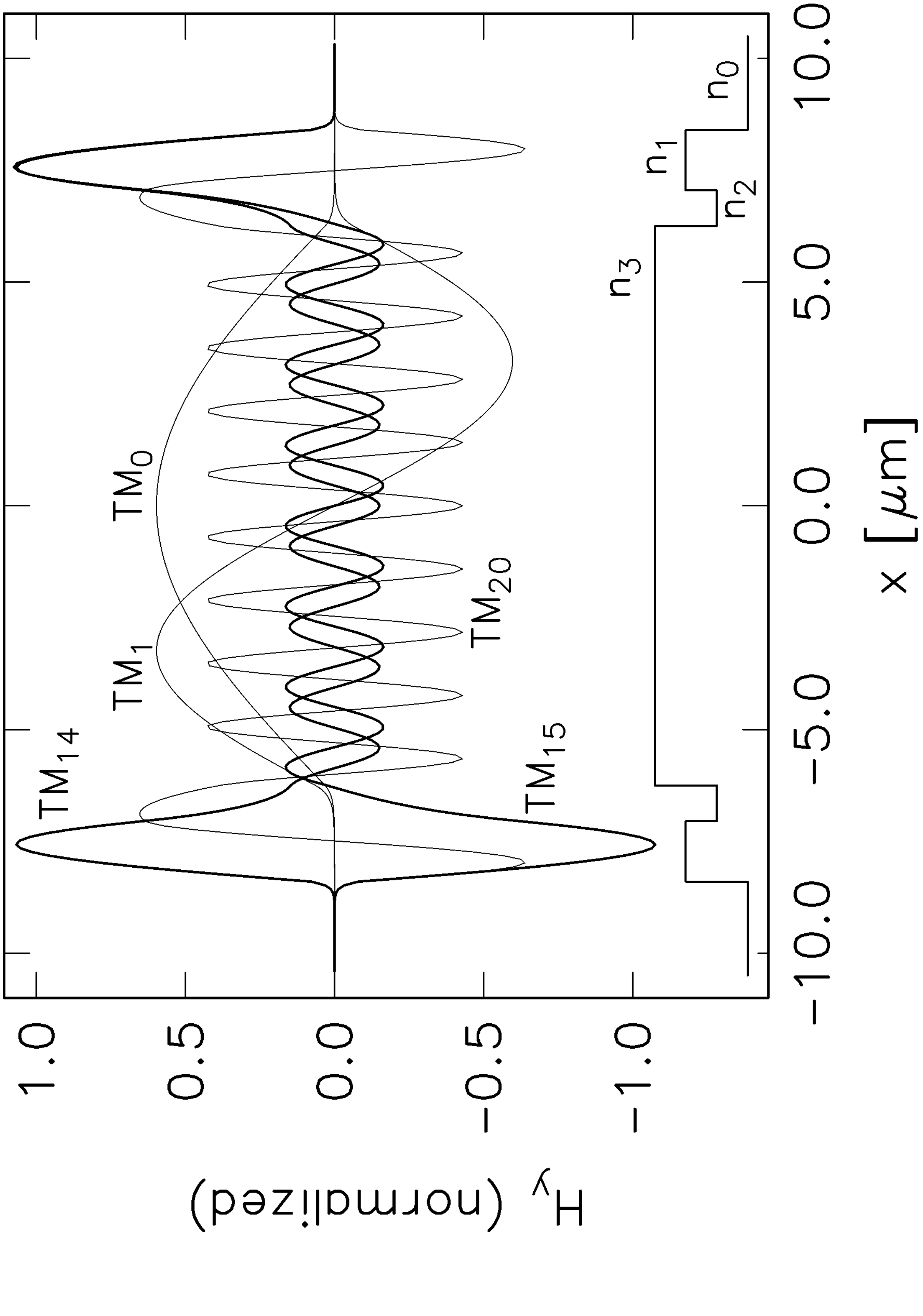
H$_y$ (normalized)
1.0
0.5
0.0
−0.5
−1.0
x [μm]
−10.0
−5.0
0.0
5.0
10.0
TM$_0$
TM$_1$
TM$_{14}$
TM$_{15}$
TM$_{20}$
n$_0$
n$_1$
n$_2$
n$_3$

Figure 3

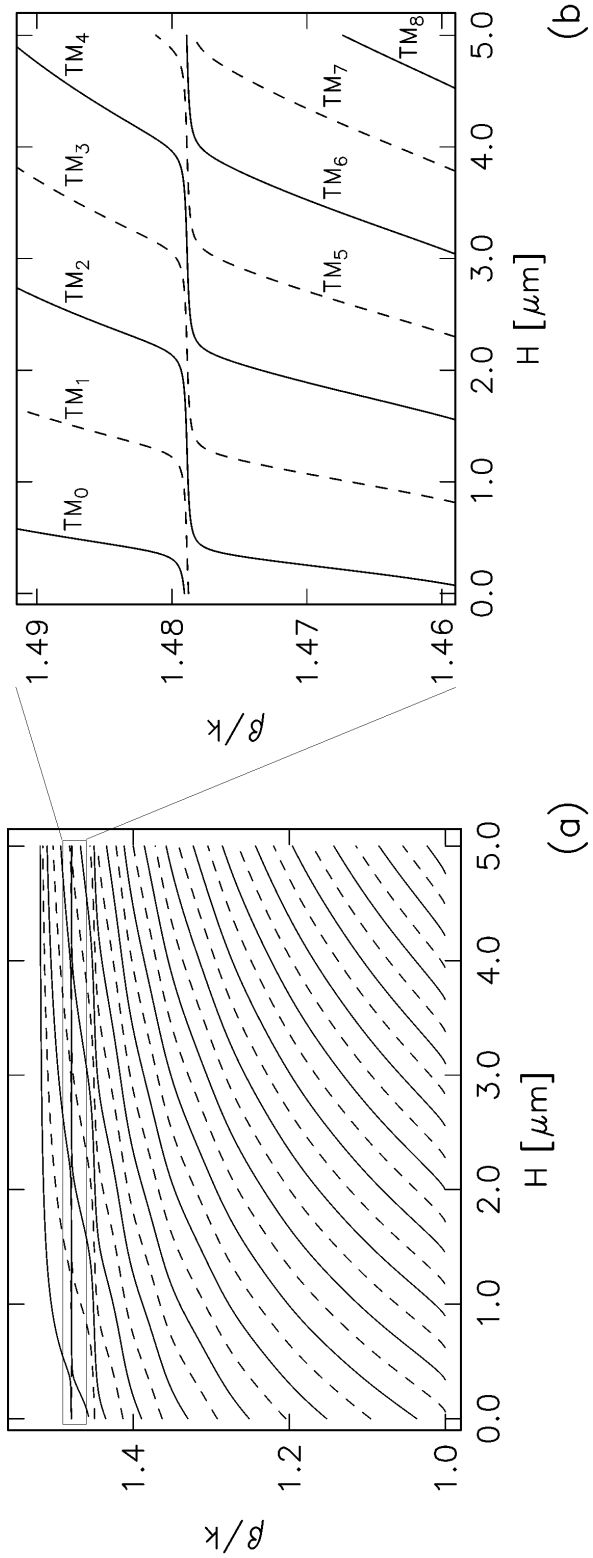

Figure 4

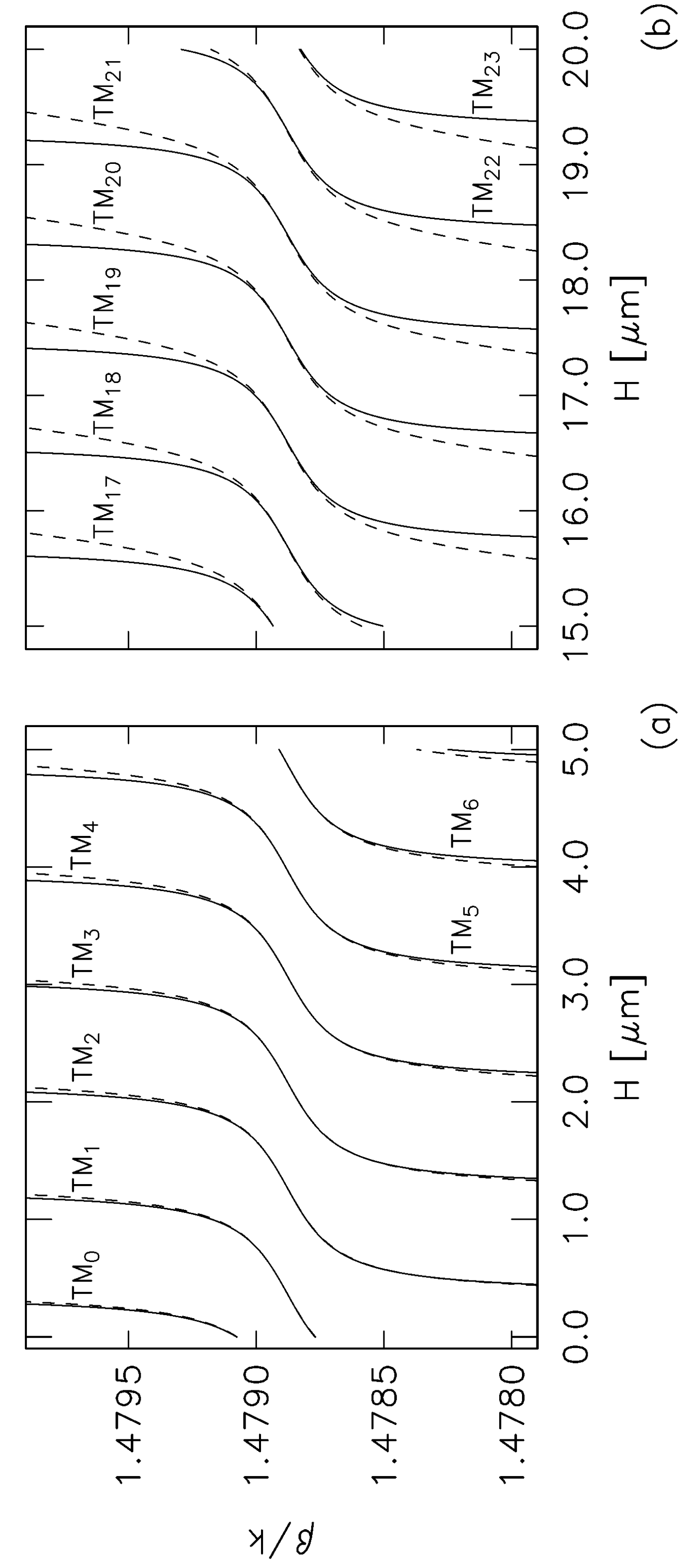

(a)
(b)
H [μm]
β/k
1.4795
1.4790
1.4785
1.4780
0.0
1.0
2.0
3.0
4.0
5.0
15.0
16.0
17.0
18.0
19.0
20.0
TM_0
TM_1
TM_2
TM_3
TM_4
TM_5
TM_6
TM_{17}
TM_{18}
TM_{19}
TM_{20}
TM_{21}
TM_{22}
TM_{23}

Figure 5

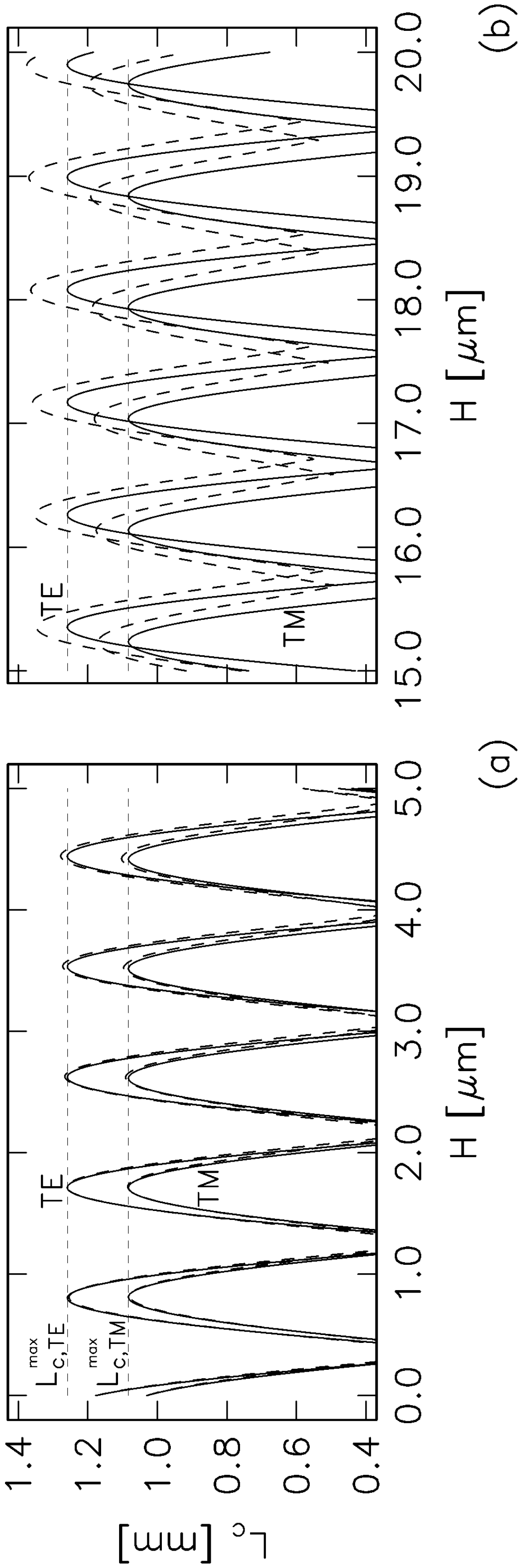

(a)
(b)
H [μm]
H [μm]
Lc [mm]
TE
TM
TE
TM
Lc,TE max
Lc,TM max
1.4
1.2
1.0
0.8
0.6
0.4
0.0
1.0
2.0
3.0
4.0
5.0
15.0
16.0
17.0
18.0
19.0
20.0

Figure 6

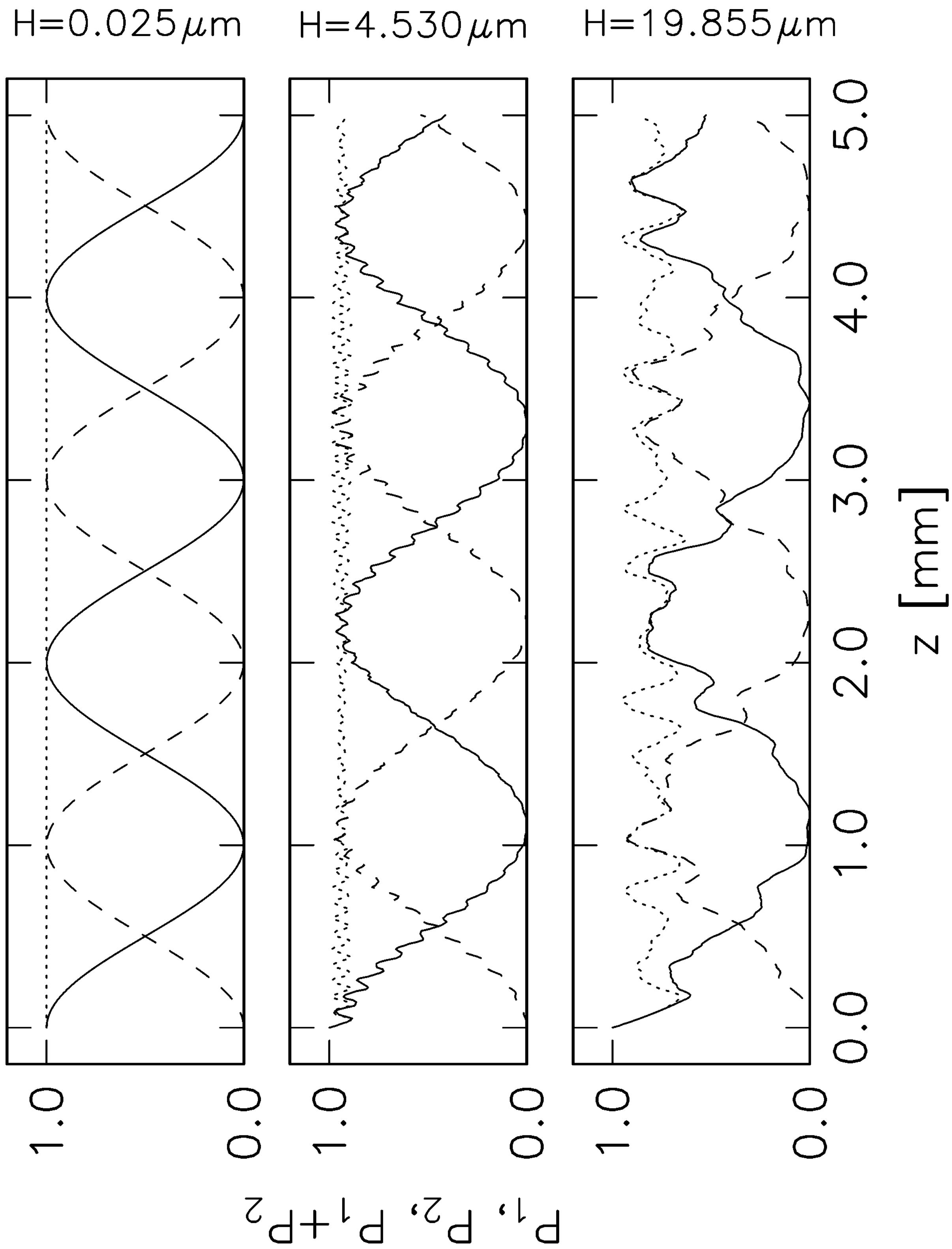

Figure 7

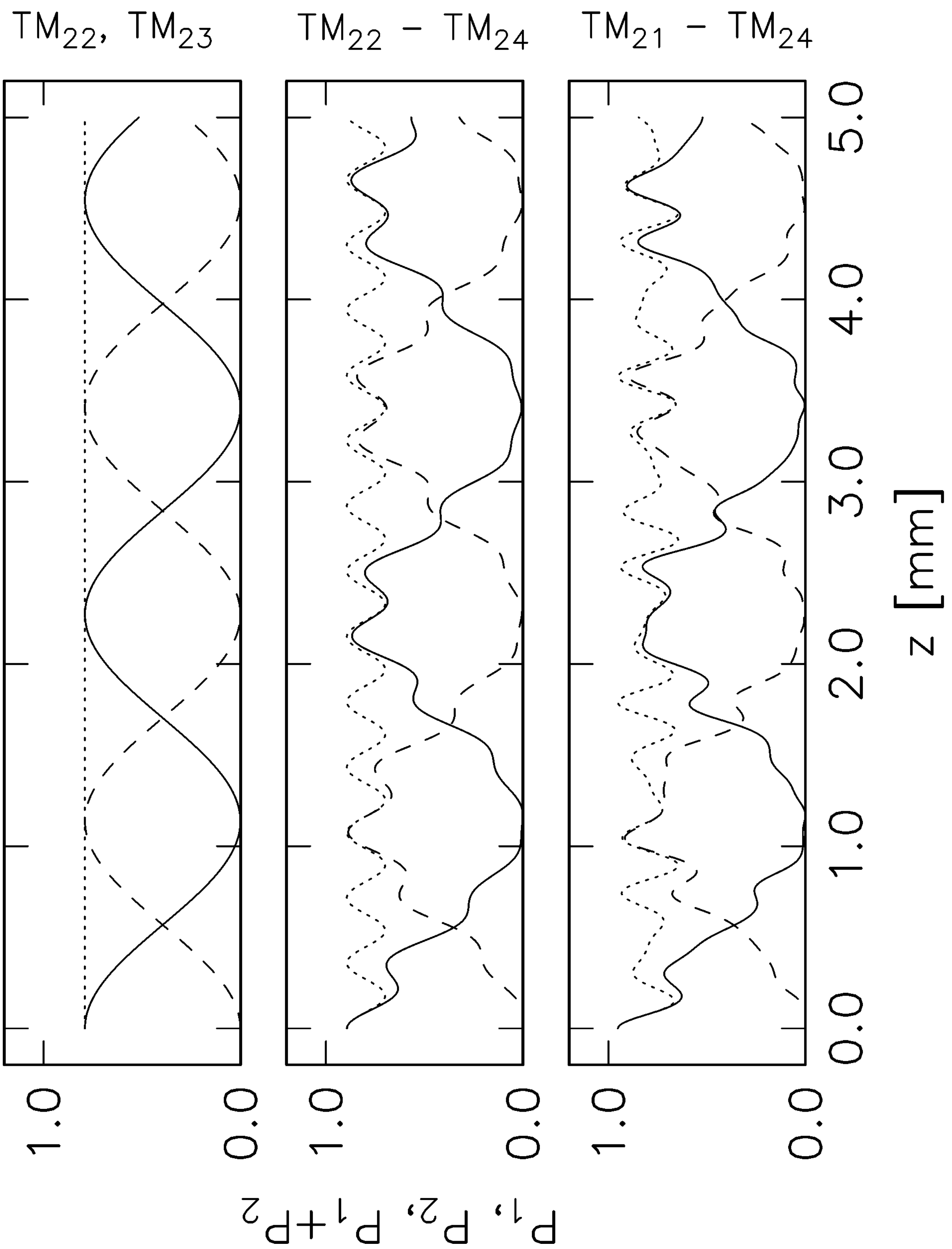

TM22, TM23
TM22 - TM24
TM21 - TM24
0.0
1.0
2.0
3.0
4.0
5.0
z [mm]
1.0
0.0
P1, P2, P1+P2

Figure 8

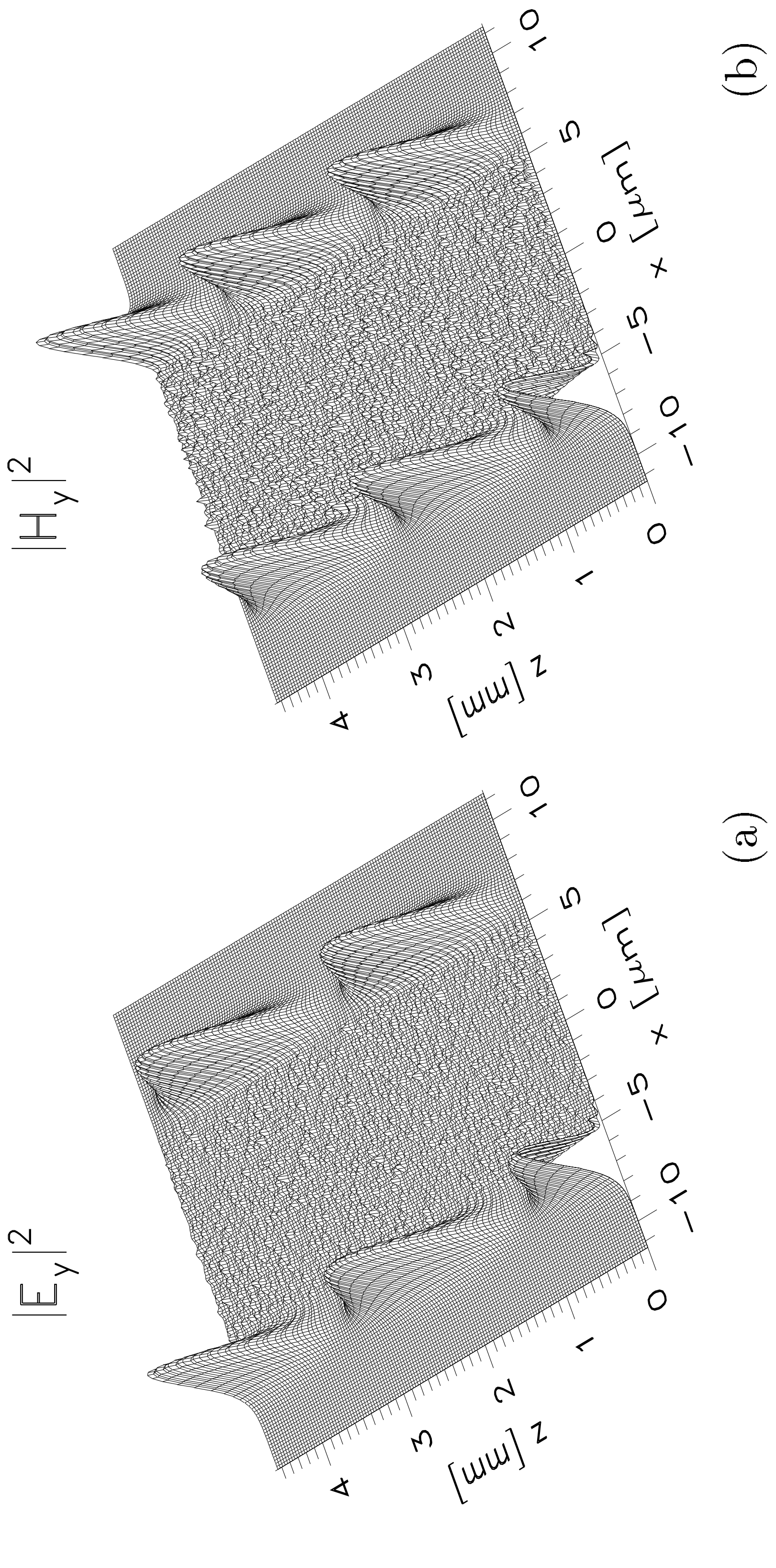

Figure 9

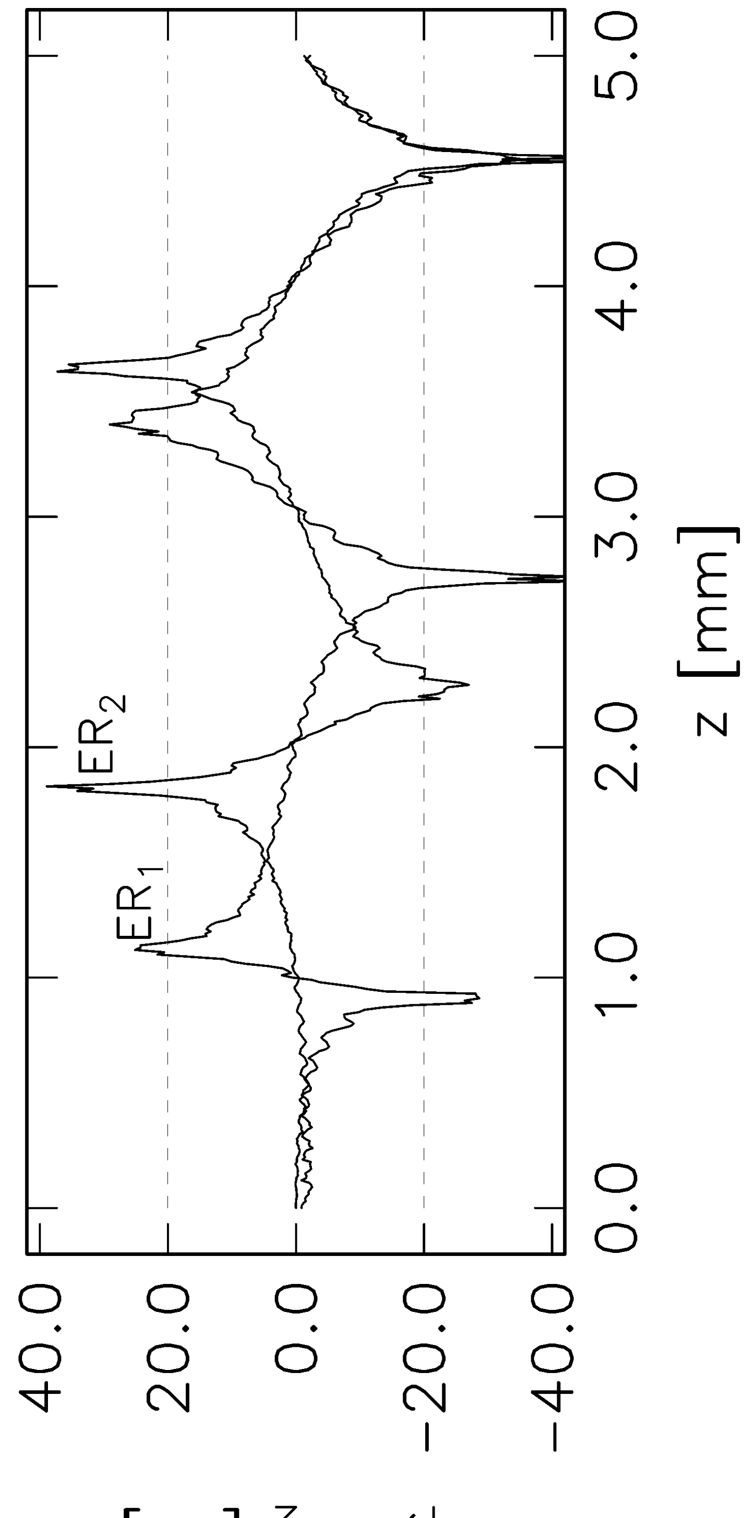

Figure 10

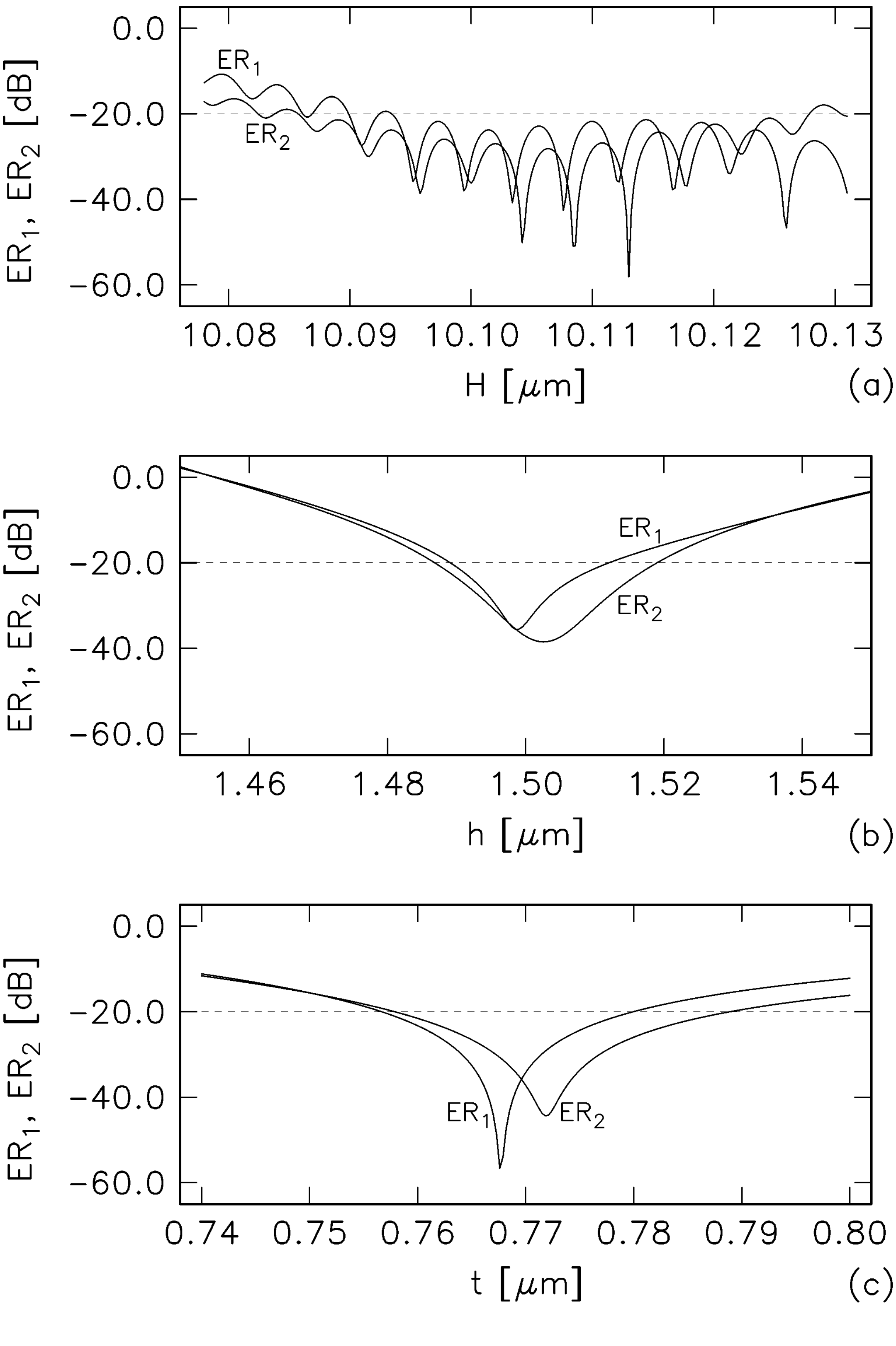
0.0
-20.0
-40.0
-60.0
ER1, ER2 [dB]
ER1
ER2
10.08
10.09
10.10
10.11
10.12
10.13
H [μm]
(a)
ER1
ER2
1.46
1.48
1.50
1.52
1.54
h [μm]
(b)
ER1
ER2
0.74
0.75
0.76
0.77
0.78
0.79
0.80
t [μm]
(c)